A linear relationship between reactivity and the reciprocal of uranium concentration in thermal spectrum molten salt reactors*

Changing Yu,[1] Guifeng Zhu,[1,2,†] Shuyang Jia,[1,3] Yang Zou,[1,2,‡] Rui Yan,[1,2] Jian Guo,[1,2] Yafen Liu,[1,2] Bo Zhou,[1,2] and Xuechao Zhao[1]

[1]*Shanghai Institute of Applied Physics, Chinese Academy of Sciences, Shanghai 201800, China*
[2]*University of Chinese Academy of Sciences, Beijing 100049, China*
[3]*ShanghaiTech University, Shanghai 201210, China*

Knowing the precise relationship between fuel loading and reactivity helps guide the smooth progress of reactor criticality extrapolation and online refueling in molten salt reactors (MSRs). This study aims to explore and explain the linear relationship between reactivity and the reciprocal of uranium concentration in thermal spectrum MSRs. By applying the neutron balance theory, we analyzed neutron absorption of neutron by various nuclides under several single lattice models with varying fuel concentrations. Our findings reveal a simple linear correlation between reactivity and the reciprocal of uranium concentration, which is successfully explained from the perspective of nuclear reaction cross-sections that adhere to the 1/v law in a thermal neutron spectrum. Furthermore, we identified the single-group neutron absorption cross-sections of structural materials and carrier salts exhibit an approximate linear relationship with the single-group fission cross-section of ^{235}U, and the reciprocal of the fission cross-section of ^{235}U exhibits an approximate linear relationship with uranium concentration. This linear relationship will deviate as the volume fraction of molten salt continues to increase since more neutrons will be captured in the resonance energy spectrum. But it remains valid within a 25% volume fraction of molten salt, and still demonstrates its broad applicability in the physical design and operation of thermal molten salt reactors.

Keywords: Molten salt reactor, Reactivity, Uranium concentration, Cross-sections, Linear

Abbreviations

k_{eff}	Effective neutron multiplication factor
ρ	Reactor reactivity
N_0	Count rate of the neutron detector before loading fuel
N	Count rate of the neutron detector after loading fuel
VF	Molten salt volume fraction
R_{f}	Fission reaction rate
R_{a}	Absorption reaction rate
R_{c}	Neutron absorption reaction rate of other materials
L	Neutron leakage rate
υ	Average number of neutrons emitted per fission
M_{i}	Atomic number densities of nuclides i
σ_a^i	Single-group fission cross-section of nuclide i
σ_f^i	Single-group absorption cross-section of nuclide i
$\bar{\sigma}$	Single-group cross-sections
E	Energy
$\phi(E)$	Neutron flux
wt	^{235}U enrichment

I. INTRODUCTION

At the Generation IV International Forum (GIF), global experts in nuclear energy systems established a consensus on fourth-generation reactor technologies, ultimately selecting six candidate designs [1, 2]. Among these, the molten salt reactor (MSR) stands out as the only liquid-fueled system, utilizing molten salt both as fuel and coolant [3–5]. This unique liquid-fuel characteristic fundamentally distinguishes its fuel-loading methodology from that of solid-fuel reactors such as pressurized water reactors (PWRs) [6–8]. In PWRs, pre-fabricated fuel assemblies are loaded into the core in discrete batches, with spatial heterogeneity intentionally introduced through varying assembly types or structural configurations [9]. In molten salt reactors, nuclear fuel is typically added to the core and uniformly distributed throughout the fuel salt loop as the fuel salt flows, ignoring temperature distribution effects [10]. During reactor loading, monitoring reactivity variation is crucial for safety. In molten salt reactors, liquid fuel characteristics lead to unique relationships between reactivity and loading.

Liquid-fueled molten salt reactors (MSRs) can be classified into two main types based on their neutron spectrum: thermal-spectrum MSRs and fast-spectrum MSRs [11]. Thermal-spectrum MSRs typically employ graphite as a moderator and fluoride salts as the fuel salt [12, 13]. In contrast, fast-spectrum MSRs lack a moderator and can utilize either fluoride or chloride salts as the fuel salt [14–16]. Additionally, there exists a unique variant of molten salt reactors that uses solid fuel while relying on liquid molten salt as the coolant [17, 18]. This design features fuel structures such as coated particle fuel pebbles or fuel rods, with physical characteristics resembling those of traditional solid-fuel reactors. It is important to note that the scope of this paper focuses exclusively on liquid-fueled MSRs and does not include this solid-fuel variant.

Research on molten salt reactors can be traced back to

* Supported by Youth Innovation Promotion Association of Chinese Academy of Sciences (No.2020261), Strategic Priority Research Program of Chinese Academy of Sciences (No.XDA02010000), Shanghai Pilot Program for Basic Research – Chinese Academy of Science, Shanghai Branch (JCYJ-SHFY-2021-003)
† Corresponding author, zhuguifeng@sinap.ac.cn
‡ Corresponding author, zouyang@sinap.ac.cn

the mid-20th century, with the most well-known example being the Molten Salt Reactor Experiment (MSRE). MSRE achieved initial criticality on June 1, 1965, making it the longest-operating molten salt reactor to date [19]. The initial loading process of MSRE can be summarized as follows: Initially, 4560 kg of carrier salt (64.75% LiF-30.09% BeF_2-5.16% ZrF_4) and 236 kg of depleted uranium feed salt (73% LiF-27% $^{238}UF_4$) are thoroughly mixed outside the reactor vessel and then transferred through piping into the reactor vessel. According to calculations, a certain amount of high-enriched uranium feed salt (73% LiF-27% UF_4, ^{235}U 93wt%) is added after being similarly mixed outside the reactor vessel and then injected into the reactor vessel. This process is repeated multiple times until extrapolated results indicate the need to add approximately 1 kg of high-enriched uranium fuel. Using the feeding port of the pump, fuel capsules containing 150 g of high-enriched uranium feed salt (73% LiF-27% UF_4, ^{235}U 93wt%) are gradually introduced. The molten salt flows out from the openings of the fuel capsules after melting at high temperatures. Through the operation of the pump, it is mixed into the fuel salt inside the reactor vessel, completing the initial critical loading process [19, 20]. Throughout the entire feeding process, the nuclear fuel is quickly and thoroughly mixed into the fuel salt system. Thus, the process effectively increases the uranium concentration in the fuel salt.

Loading nuclear fuel and achieving initial criticality of the reactor is the most crucial step before reactor power operation, ensuring the its safety and controllability. During the loading and criticality extrapolation processes, establishing the relationship between reactivity and the amount of nuclear fuel loaded is the physical basis for designing loading schemes. The reciprocal neutron count rate extrapolation method is commonly used for extrapolating critical loading [21]. The method involves plotting the reciprocal of the neutron counting rate against the loading amount of nuclear fuel. Extrapolating this curve to the point where it intersects the horizontal axis allows estimation of the loading amount required to achieve criticality. The physical principle of this method is based on the source multiplication theory [22]. According to the source multiplication theory, the effective neutron multiplication factor k_{eff} can be approximated as:

$$k_{\text{eff}} = 1 - \frac{N_0}{N} \tag{1}$$

In the equation, N_0 represents the count rate of the neutron detector before loading nuclear fuel into the reactor, and N represents the count rate of the neutron detector after loading a certain amount of nuclear fuel. As more nuclear fuel is loaded into the reactor, the corresponding neutron count rate (N) increases. As the reactor approaches criticality, k_{eff} approaches 1, and the corresponding neutron count rate N tends towards infinity. The reciprocal extrapolation method of neutron count rate approximates a linear relationship between k_{eff} and the amount of fuel loaded. The curve typically exhibits concavity because this proportional relationship is a conservative approximation, as the amount of nuclear fuel loading increases, the reactivity introduced per unit of nuclear fuel loading decreases. While conservative approximations are generally beneficial for reactor criticality safety, they can sometimes lead to disadvantageous judgments about the reactor's status.

In the realm of nuclear reactor physics, particularly during the startup process, the measurement of reactivity stands as a primary means to characterize the reactor's status. The methods for measuring reactivity mainly include the source multiplication method [23, 24], the inverse kinetics method [25], and the period method [26]. Although these methods are also applicable to liquid-fuel molten salt reactors, they face similar challenges. All of these methods require processing neutron signals captured by neutron detectors to obtain reactivity parameters. Due to factors such as the influence of external neutron source worth and the spatial effects of control rods, these measurement methods encounter considerable difficulties in achieving precise measurements under subcritical conditions. In order to obtain more precise measurement results, some scholars have to resort to complex correction methods based on theoretical calculations [27, 28]. If the relationship between reactivity and nuclear fuel loading can be determined, it would allow for direct calculation of reactor reactivity based on the amount of fuel loaded.

Due to the liquid fuel characteristics of molten salt reactors, the reactor can achieve online refueling during operation [5, 29]. Compensate for the decreased reactivity due to burnup by online refueling. Currently, the online refueling process is primarily simulated through coupled neutron transport and burnup code. In simulation calculations, the adjustment of the nuclear fuel addition rate is typically used to achieve k_{eff} regulation. The methods used include secant method [30], linear approximations of k_{eff} with burnup depth or fuel addition rate [31]. These methods typically require multiple iterations of neutron transport calculations to update the feed rate of nuclear fuel.

Therefore, establishing a relationship between reactivity and nuclear fuel loading is not only crucial for reactivity measurement but also serves as a key guiding principle for the entire process of fuel loading, critical extrapolation, and criticality search calculations related to fuel addition. It is widely recognized that reactivity and the amount of nuclear fuel loaded exhibit a complex nonlinear relationship [32], making it generally difficult to establish a simple theoretical relationship. However, as mentioned earlier, the fuel-loading process in a molten salt reactor primarily involves increasing the uranium (or other nuclear fuel) concentration in the fuel salt without altering the reactor's structural configuration. Therefore, for molten salt reactors, under consistent operational conditions, a corresponding relationship should exist between the uranium concentration in the fuel salt and the reactor's reactivity. Building on this concept, through an analysis of the relationship between k_{eff} and uranium concentration, we have identified a highly linear correlation between reactivity and the reciprocal of uranium concentration. Further investigation is required to explore the theoretical foundation and applicability of this linear relationship.

Therefore, the objective of this paper is to theoretically establish and validate the relationship between uranium concen-

tration in molten salt reactor fuel salts and reactivity, with a focus on the principles and applicability of the linear relationship. The main research content is structured as follows, section 2 introduces the reactor model. Section 3 describes the discovery process of the linear relationship between $1/k_{\text{eff}}$ and the reciprocal of uranium concentration. Section 4 focuses on principle verification. Based on the graphite-moderated single-lattice model and neutron balance theory, the relationship between k_{eff} and uranium concentration is solved step by step, establishing a theoretical explanation for the linear relationship between the reciprocal of k_{eff} and the reciprocal of uranium concentration. Section 5 verifies the applicability of the linear relationship. Using the graphite-moderated core model, the verification is extended to a broader range of fuel loading conditions, as well as scenarios involving different molten salt volume fractions (VF), uranium enrichment levels, and ^{232}Th/^{233}U fuel. Section 6 summarizes and discusses the findings of this paper.

II. REACTOR MODEL

The study focuses on the relationship between reactor reactivity and uranium concentration in molten salt reactors, using a graphite moderation model as the subject of investigation. The reactor core utilizes graphite as a moderator and consists primarily of fuel salt channels, graphite moderators, graphite reflectors, and reactor vessel, etc., as shown in Fig. 1. The lattice structure is hexagonal prismatic, with a salt volume fraction of 15%, meaning that the fuel salt occupies 15% of the total volume. The core active region has consistent dimensions of 200 cm in diameter and height. The moderator and reflector graphite have a density of 2.3 g/cm^3, with a reflector thickness of 30 cm. The reactor operates with a fuel salt composed of 67LiF-33BeF_2-xUF_4(mol%). After adjusting the value of x, normalize the composition of the fuel salt. Additionally, the fuel salt may include a certain proportion of ThF_4 to simulate thorium loading, which will be further analyzed in Section 5.4. The density of molten salts is calculated from the densities of unit salts [33] by volume-weighted average [34]. The accuracy of this method, based on average molar volume, is within 3% [35]. The parameters of the fuel salt are shown in Table 1.

TABLE 1. Fuel salt parameters.

Parameters	Value
Fuel salt(mol%)	67LiF-33BeF_2-xUF_4
Temperature	900 K
Salt density (g/cm^3)	LiF: 1.81-0.00049·(T-848.2)
	BeF_2: 1.96-0.000015·(T-552)
	UF_4: 6.485-0.00092·(T-1036)
	ThF_4: 6.058-0.000759·(T-1110)
^{7}Li abundance	99.95 at%
^{235}U enrichment	20 wt%

The theoretical analysis, based on the single-lattice model, and its validation within the core model are derived from simulations conducted using the CSAS6 module in SCALE6.1 [36]. The CSAS6 module combines a cross-section processing module with a three-dimensional Monte Carlo transport code to perform criticality analysis. Specifically, BONAMI is utilized to process cross sections in the unresolved resonance energy region, while CENTRM/PMC handles those in the resolved resonance energy region. The transport calculations are executed using KENO-VI. CSAS6 provides critical outputs such as k_{eff}, neutron energy spectra, and single-group cross sections for various fuel compositions. In this study, the criticality calculations are performed with 20,000 particles, and the 238-group ENDF/B-VII.0 library is selected as the database.

III. THE DISCOVERY OF THE LINEAR RELATIONSHIP

Prior to the study presented in this paper, initial research focused on the reactor loading and criticality extrapolation process, based on the reactor model illustrated in Fig. 1(a). The study particularly emphasized reactivity calculations during the loading process. As previously mentioned, the simulation involves incrementally increasing the mole percentage of UF_4 in the fuel composition 67LiF-33BeF_2-xUF_4 (mol%), where x represents the amount of UF_4. Due to the liquid fuel characteristics of the molten salt reactor, each batch of nuclear fuel, once added, is rapidly mixed and uniformly distributed throughout the entire fuel channels of the reactor [37, 38]. Consequently, there is a direct relationship between the reactivity of the reactor and the amount of fuel added, eliminating the need to consider the spatial arrangement of fuel as required in pressurized water reactors. Simulations using SCALE 6.1 can determine the k_{eff} after each batch of nuclear fuel is added to the reactor, and efforts are made to identify the relationship between the uranium concentration in the fuel salt or uranium loading and k_{eff}. During the extrapolation process for fuel addition, a practical approximation is employed, assuming that the increase in k_{eff} is linearly related to the amount of fuel added. Therefore, the study initially analyzes the relationship between k_{eff} and the concentration of ^{235}U, as shown in Fig. 2(a). Here, M_{U-235} refers to the atomic number density of ^{235}U in the fuel salt (units: atoms/b-cm). It is observed that the relationship between k_{eff} and M_{U-235} follows a concave curve, which only approximates a linear relationship when k_{eff} approaches 1.

To establish the relationship between k_{eff} and M_{U-235}, neutron balance theory is utilized for analysis. According to this theory, the effective multiplication factor k_{eff} of a reactor system can be defined as the ratio of neutron production rate to neutron loss rate [39]:

$$k_{\text{eff}} = \frac{\text{neutron production rate}}{\text{neutron loss rate}(absorption + leakage)} \tag{2}$$

The effective multiplication factor k_{eff} is influenced by the system's material composition, structure, and the neutron leakage. The mathematical expression is written as follows:

$$k_{\text{eff}} = \frac{\nu R_f}{R_a + L} \tag{3}$$

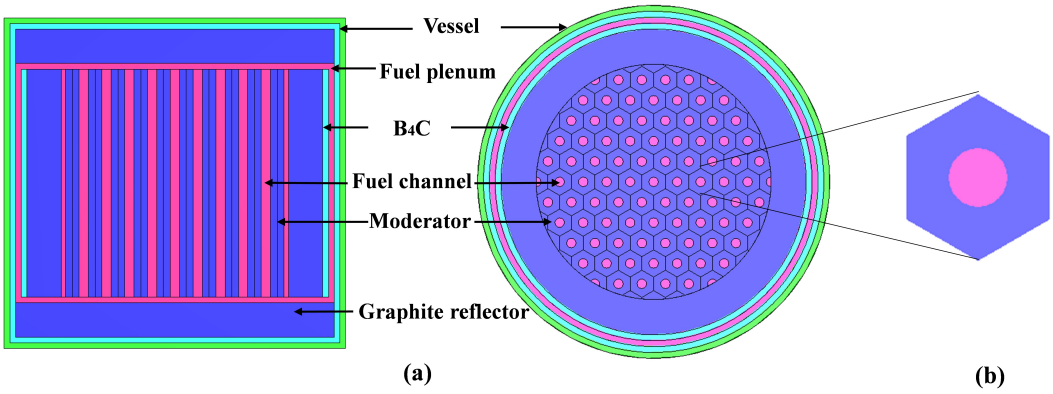

Fig. 1. (Color online) Schematic diagram of the reactor core model(a) and the single-lattice model(b).

In Eq. (3), ν represents the average number of neutrons emmited per fission,R_f is the fission reaction rate, R_a is the total absorption reaction rate, which includes fuel salt, graphite, and structural materials, and L is the neutron leakage rate. Eq. (3) involves the solution of neutron flux and reaction cross-sections, necessitating neutron transport calculations. From a qualitative perspective, the reaction rate of uranium is directly proportional to the concentration of ^{235}U. Furthermore, assuming that the neutron absorption reaction rate R_c of materials other than uranium isotopes remains constant, then Eq. (3) can be approximated and rewritten as:

$$k_{\text{eff}} = \frac{c_{01} M_{\text{U}-235} \nu}{c_{02} M_{\text{U}-235} + R_c + L} \tag{4}$$

In Eq. (4), c_{01} and c_{02} are both constants. If we take the reciprocal of both sides of Eq. (4), and assume that ν and L are also constants, it can be rewritten in the following form:

$$\frac{1}{k_{\text{eff}}} = a \cdot \frac{1}{M_{\text{U}-235}} + b \tag{5}$$

Eq. (5) suggests that $1/k_{\text{eff}}$ may exhibit an approximate linear relationship with $1/\text{M}_{\text{U}-235}$. To verify the validity of Eq. (5), Fig. 2(a) is modified by swapping the horizontal axis to $1/\text{M}_{\text{U}-235}$ and the vertical axis to $1/k_{\text{eff}}$, as shown in Fig. 2(b). A linear fit is performed on $1/k_{\text{eff}}$ and $1/\text{M}_{\text{U}-235}$, with a linear determination coefficient R^2 as high as 0.99997. Therefore, although Eq. (5) is derived from a rough qualitative analysis of Eq. (3), the results shown in Fig. 2(b) suggest the possibility that Eq. (5) is valid. Eq. (5) indicates that the reactivity of the reactor can be quickly obtained through the uranium loading or uranium concentration, which would be a beneficial discovery in the process of reactor loading.

Due to the liquid fuel characteristics of molten salt reactors, the loading of nuclear fuel is equivalent to increasing the uranium concentration in the fuel salt. Based on the qualitative analysis from Eq. (2) to Eq. (5), as well as the linear regression analysis of Fig. 2(b), we have discovered that the reactivity of the reactor or $1/k_{\text{eff}}$ exhibits a linear relationship with the reciprocal of the uranium concentration. However, during the actual fuel loading process, the neutron absorption reaction cross-sections of various nuclides within the reactor are changing, and the assumption in Eq. (4) that c_{01}, c_{02}, and R_c are constants may not hold true, necessitating further research.

Moving forward, this paper utilizes neutron balance theory to examine the neutron energy spectrum and reaction cross-section variations in response to changes in uranium concentration. It progressively solves Eq. (3) and theoretically validates the linear relationship proposed in Eq. (5).

IV. PRINCIPLE VALIDATION

To investigate the relationship between reactivity and uranium concentration using neutron balance theory, we utilize the single lattice cell model illustrated in Fig. 1(b). The hexagonal single lattice model features a central channel for the fuel salt, surrounded by a graphite moderator. This simplified model omits intricate core configurations, thereby eliminating the need to account for neutron absorption by structural materials [40, 41]. Additionally, to neglect the influence of neutron leakage, a white reflective boundary condition is applied to the single lattice structure. During calculations in SCALE 6.1, the concentration range of UF_4 is 0.02-1 mol%, corresponding to a k_{eff} range of 0.12-1.42, ensuring a sufficiently broad scope for analysis. Consequently, the neutron absorption reaction in Eq. (3) includes only the fuel salt and graphite moderator materials, with a leakage rate(L) equal to zero. The equation can be further expanded as:

$$k_{\text{eff}} = \frac{\nu(\sigma_f^{\text{U}-235} M_{\text{U}-235} + \sigma_f^{\text{U}-238} M_{\text{U}-238})}{(\sigma_a^{\text{U}-235} M_{\text{U}-235} + \sigma_a^{\text{U}-238} M_{\text{U}-238} + \sum \sigma_a^i M_i)} \tag{6}$$

In the equation, $\sigma_f^{\text{U}-235}$, $\sigma_f^{\text{U}-238}$, $\sigma_a^{\text{U}-235}$, $\sigma_a^{\text{U}-238}$, $\text{M}_{\text{U}-235}$, and $\text{M}_{\text{U}-238}$ respectively denote the microscopic single-group cross sections for fission and absorption of ^{235}U and ^{238}U, as well as their atomic number densities. The terms σ_a^i and M_i correspond to the single-group absorption cross-sections and the atomic number densities of nuclides other than ^{235}U and ^{238}U, where i includes ^{6}Li, ^{7}Li, ^{9}Be, ^{19}F, and

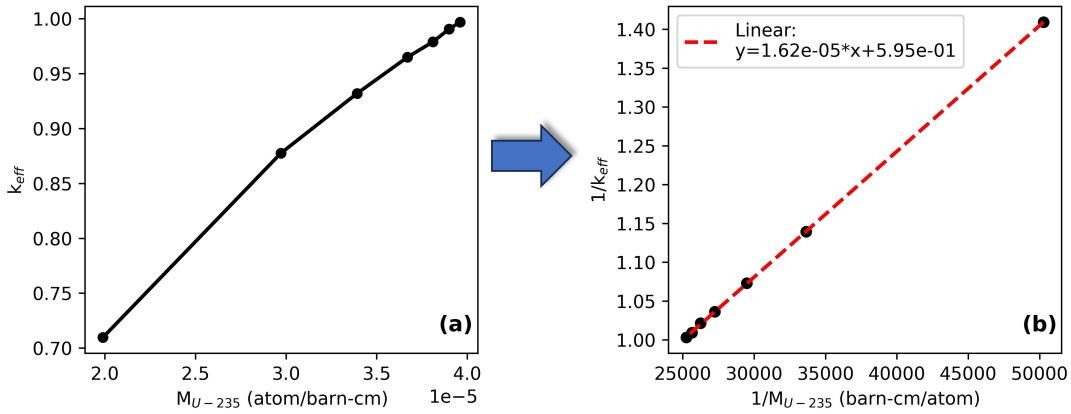

Fig. 2. (Color online) Relationship between k_{eff} and uranium concentration, the curve relationship between k_{eff} and M_{U-235} (a), $1/k_{\text{eff}}$ exhibits a linear relationship with $1/M_{U-235}$ (b).

^{12}C. Due to the approximate proportionality between the average neutron flux density in the graphite moderation region and the fuel region, the single-group cross-section of ^{12}C underwent neutron flux equivalence treatment.

Upon careful observation of Eq. (6), the enrichment of ^{235}U is 20 wt%, and there is a fixed proportional relationship between M_{U-235} and M_{U-238}. Additionally, during the fuel loading process, changes in the concentrations of other nuclides in the fuel salt can be considered negligible aside from uranium. Regarding the average number of fission neutrons (ν), since the fissile material is uranium with fixed enrichment, it also approximates a constant. Therefore, the primary variables on the right-hand side of the equation are the single-group cross-sections of each nuclide and the uranium concentration. Next, we examine the variation of single-group cross-sections with uranium concentration, incorporating the neutron energy spectrum, and gradually simplify Eq. (6) accordingly.

A. Variations in energy spectrum and cross-sections

The single-group cross-sections are primarily related to the neutron energy spectrum, calculated as follows:

$$\bar{\sigma} = \frac{\int \sigma(E)\phi(E)\,dE}{\int \phi(E)\,dE} \tag{7}$$

Here, $\sigma(E)$ represents the nuclear reaction cross-section for energy distribution. This value remains constant for a given nuclide and type of reaction. $\phi(E)$ represents the neutron flux distribution in the region where the nuclide is present, i.e., the neutron energy spectrum. The neutron energy spectrum is influenced by various factors such as reactor structure, uranium concentration, and temperature. It is a result of neutron transport and can be calculated using the SCALE 6.1 program.

Fig. 3(a) shows the normalized neutron energy spectra in the fuel region at different uranium concentrations, along with the cross-sections of key neutron absorption reactions in a single lattice. For fissionable isotopes, the primary neutron absorption reactions of ^{235}U and ^{238}U are fission (n, f) and capture (n, γ) reactions, respectively. The primary reaction type for ^{6}Li is tritium production through the (n, T) reaction. The main nuclear reaction type for other light nuclei is capture absorption (n, γ) reactions. Additionally, for the nuclides ^{9}Be and ^{19}F, there is also a significant proportion of (n, α) absorption reactions in the high-energy region, which absorb neutrons to produce ^{4}He particles. Upon observation, it is noted that although the neutron flux decreases in the thermal neutron region (E $<$ 1 eV) with increasing uranium concentration, there is a corresponding increase in other energy regions. However, overall, the neutron flux in the thermal neutron region remains significantly higher compared to the fast neutron region, indicating a predominantly thermal neutron spectrum. Furthermore, although the neutron flux in different energy regions varies with uranium concentration, the overall shape characteristics of the spectrum remain essentially unchanged. Observe the variation of reaction cross-sections for major nuclides with energy in Fig. 3(a). For the two fissionable nuclides, ^{235}U and ^{238}U, their fission and capture cross-sections in the thermal neutron region both follow the 1/v law, meaning $\sigma(E)$ is proportional to $1/\sqrt{E}$. In the intermediate energy region, they exhibit strong resonance peaks, particularly noticeable in the case of ^{238}U. Other light nuclei's neutron absorption cross-sections, except for the reactions ^{9}Be(n, α) and ^{19}F(n, α), follow the 1/v law in larger energy ranges.

Based on the analysis of neutron energy spectrum and neutron absorption reaction cross-sections, the following three facts can be drawn:

1. The neutron energy spectrum is a thermal neutron spectrum, where the thermal neutron flux (E $<$ 1 eV) is significantly higher than other neutron flux.

2. The neutron absorption cross-sections of major nuclides in the thermal neutron energy region follow the 1/v law, meaning $\sigma(E)$ is proportional to $1/\sqrt{E}$.

3. In the high-energy neutron range, isotopes such as ^{235}U, ^{238}U, and ^{19}F exhibit prominent resonance ab-

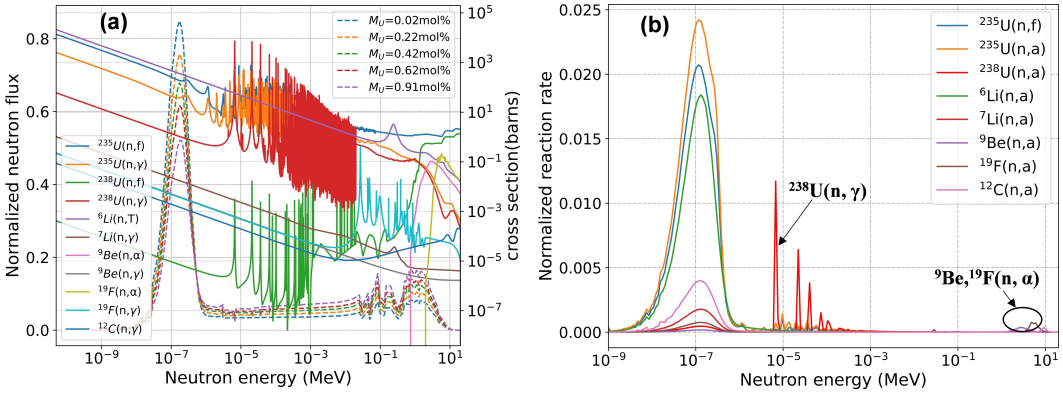

Fig. 3. (Color online) Neutron energy spectrum and cross-sections of major nuclides(a), distribution of normalized reaction rates with energy(b).

sorption peaks. Additionally, ^{9}Be and ^{19}F have significant (n,α) neutron absorption cross-sections in the fast neutron energy range.

Based on the three main facts above and Eq. (7), we can qualitatively infer that the single-group neutron absorption cross-sections of major nuclides may exhibit an approximate linear relationship with the single-group fission cross-section of ^{235}U. However, due to strong resonance absorption peaks in isotopes such as ^{235}U and ^{238}U, as well as (n,α) reactions in ^{9}Be and ^{19}F, deviations from a linear relationship may occur. To further illustrate this issue, Fig. 3(b) shows the normalized neutron reaction rates versus energy distribution curves for major nuclides under critical conditions, with uranium comprising 0.36 mol%. From Fig. 3(b), it can be seen that in the thermal neutron energy region (E $<$ 1 eV), the neutron reaction rates of the major nuclides are ranked as follows: $^{235}\mathrm{U}(n,\alpha) > ^{235}\mathrm{U}(n,f) > ^{6}\mathrm{Li}(n,\alpha) > ^{12}\mathrm{C}(n,\alpha) > ^{7}\mathrm{Li}(n,\alpha) > ^{19}\mathrm{F}(n,\alpha) > ^{238}\mathrm{U}(n,\alpha) > ^{9}\mathrm{Be}(n,\alpha)$. For major nuclides such as ^{235}U, ^{6}Li, ^{12}C, and ^{7}Li, the neutron absorption reaction rates are significantly higher in the thermal neutron region compared to other energy ranges. When calculating k_{eff} using Eq. (6), it is essential to consider primarily the neutron reaction rates in the thermal neutron region. In the resonance energy region, both ^{238}U and ^{235}U exhibit significant absorption reactions. For ^{238}U, resonant absorption in the energy range of 1 eV to 1 keV constitutes approximately 75% of its total absorption, yet this accounts for only about 2% of the overall material absorption. In addition, due to the (n,α) reactions of ^{9}Be and ^{19}F, these two nuclides have a certain proportion of neutron absorption reaction rates in the fast neutron energy region, accounting for approximately 45% and 19% of their total absorption, respectively. However, these reaction rates are significantly smaller than the absorption reaction rates of nuclides such as ^{235}U and ^{6}Li in the thermal neutron region. Therefore, for several nuclides that contribute significantly to neutron absorption reactivity, the focus is primarily on thermal neutron absorption reactions, where the neutron absorption cross-sections follow the 1/v law. Although some nuclides also contribute to neutron absorption reactions in the resonance energy region and fast neutron energy region, these contributions are relatively small.

To verify the above analysis, we use SCALE 6.1 to calculate the single-group neutron absorption cross-sections for major nuclides and analyze their linear relationships with the ^{235}U fission cross-section. Fig. 4 shows the linear relationship between the single-group neutron absorption cross-sections of ^{235}U, ^{238}U, ^{6}Li, ^{7}Li, ^{9}Be, ^{19}F, and ^{12}C, relative to the single-group fission cross-section of ^{235}U. The corresponding coefficient of determination (R^2) for each linear fit is provided. Fig. 4 demonstrates that the neutron absorption cross-sections of various nuclides show a strong linear relationship with the fission cross-section of ^{235}U. This linear relationship can be summarized as follows:

$$\sigma_a^i = c_1^i \sigma_f^{\mathrm{U}-235} + c_2^i \tag{8}$$

In the equation, σ_a^i represents the single-group neutron absorption cross-section of nuclide i, $\sigma_f^{\mathrm{U}-235}$ denotes the single-group fission cross-section of ^{235}U, where c_1^i and c_2^i represent the slope and intercept of the linear fit for nuclide i, which includes nuclides ^{235}U, ^{238}U, ^{6}Li, ^{7}Li, ^{9}Be, ^{19}F, and ^{12}C. Meanwhile, Fig. 4 shows that the coefficient of determination (R^2) for the nuclides ^{238}U and ^{9}Be is relatively smaller. This is primarily due to ^{238}U exhibiting a strong resonance absorption peak in the intermediate neutron energy region, and the nuclide ^{9}Be has a relatively large (n,α) absorption cross-section in the fast neutron energy region, as depicted in Fig. 3(a) or Fig. 3(b). An increase in uranium concentration results in a harder neutron energy spectrum, enhancing resonance and (n,α) absorption, thereby deviating from the linear relationship. However, since the single-group neutron absorption cross-sections of these nuclides are significantly smaller compared to major nuclides like ^{235}U and ^{6}Li, the use of Eq. (8) for linear approximation processing will not greatly affect the calculation of k_{eff} in Eq. (6).

Thus, we can convert all single-group absorption cross-sections in Eq. (6) into the fission cross-section of ^{235}U. Therefore, Eq. (6) can be further simplified to:

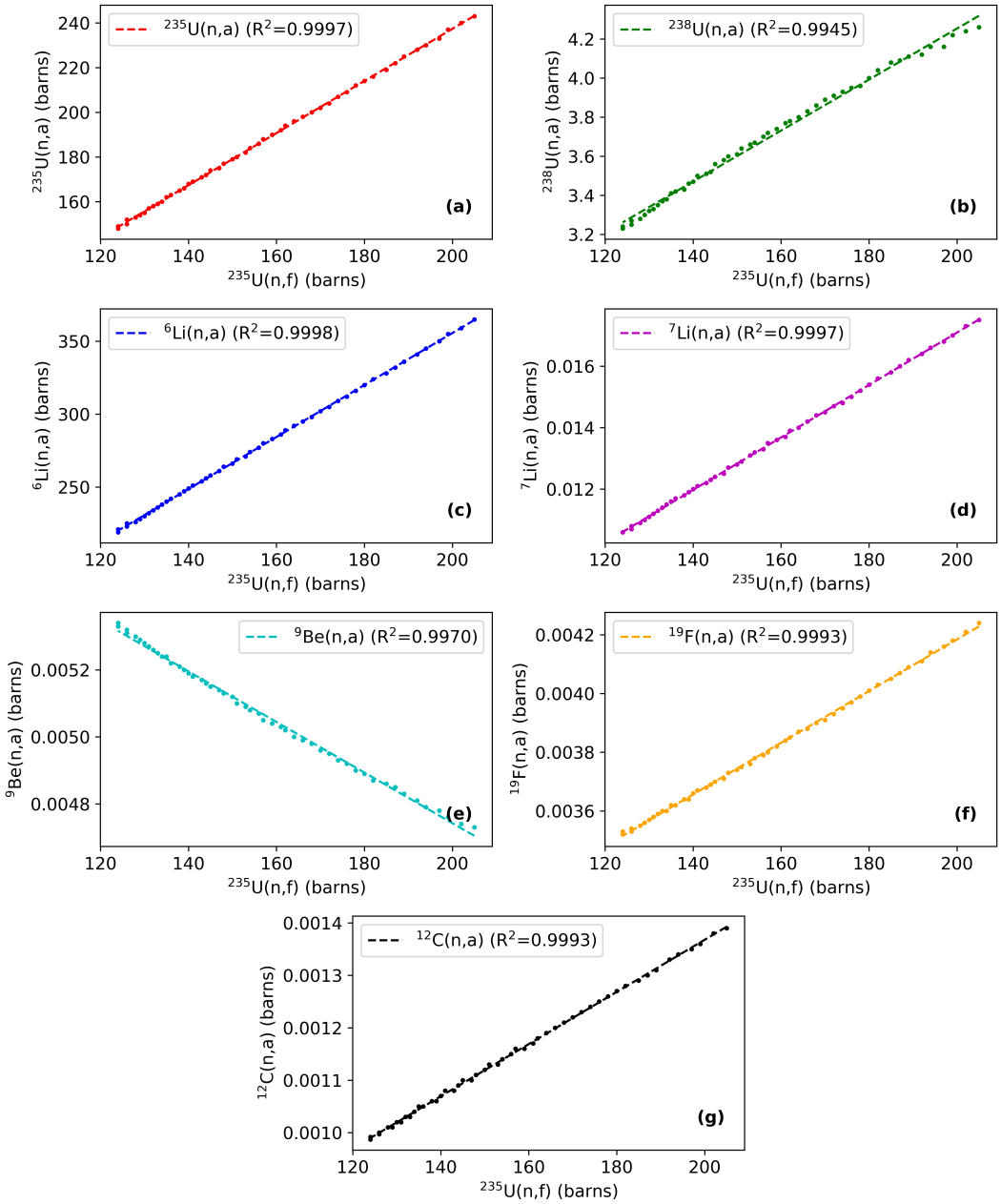

Fig. 4. (Color online) Linear fit of neutron absorption cross sections in major nuclides to ^{235}U fission cross section

$$k_{\text{eff}} = \frac{\nu(\sigma_f^{\text{U}-235} M_{\text{U}-235} + \sigma_f^{\text{U}-238} M_{\text{U}-238})}{(c_1^{\text{U}-235} + w c_1^{\text{U}-238})\sigma_f^{\text{U}-235} M_{\text{U}-235} + \sum c_1^i M_i \sigma_f^{\text{U}-235} + (c_2^{\text{U}-235} + c_2^{\text{U}-238} w) M_{\text{U}-235} + \sum c_2^i M_i}, \qquad (9)$$
$$w = \frac{(1-wt)\times 235}{wt \times 238}$$

wt represents the enrichment of ^{235}U. Meanwhile, as shown in Fig. 3(a), the fission cross-section of ^{238}U is lower by four orders of magnitude compared to that of ^{235}U. Therefore, an approximate treatment can neglect the contribution of ^{238}U's fission. Moreover, compared to the fission cross-section of ^{235}U, the intercept of the linear fit of the absorption cross-sections of ^{235}U and ^{238}U amounts to approximately 1% of $\sigma_f^{\text{U}-235}$, which can be neglected. The linear relationship between the absorption cross-sections of ^{235}U and ^{238}U and the

fission cross-section of ^{235}U are approximately proportional. Therefore, Eq. (9) can be further simplified to:

$$k_{\text{eff}} = \frac{\nu\sigma_f^{\text{U}-235} M_{\text{U}-235}}{(c_1^{\text{U}-235} + wc_1^{\text{U}-238})\sigma_f^{\text{U}-235} M_{\text{U}-235} + \sum c_1^i M_i \sigma_f^{\text{U}-235} + \sum c_2^i M_i} \tag{10}$$

In Eq. (10), the slopes c_1^i and intercepts c_2^i associated with the linear fit, where i includes ^{235}U and ^{238}U, along with other nuclides, as well as M_i, are constants. Thus, k_{eff} has been simplified to depend solely on the fission cross section $\sigma_f^{\text{U}-235}$ of ^{235}U and its concentration $M_{\text{U}-235}$. Next, by analyzing the relationship between the fission cross-section σ_f^{U-235} and the concentration $M_{\text{U}-235}$, Eq. (10) will be further streamlined.

B. Relationship between fission cross-section and uranium concentration

In Eq. (6), we express k_{eff} as a function of cross-sections and nuclide concentrations, and establish the relationship between neutron absorption cross-sections in various nuclides and the fission cross-section of ^{235}U in Eq. (8). Therefore, under the condition where the concentration of non-fissile nuclides is approximately constant, there are currently two quantities related to k_{eff} on the right side of Eq. (10), which are $M_{\text{U}-235}$ and $\sigma_f^{\text{U}-235}$. Next, we further establish the relationship between $M_{\text{U}-235}$ and $\sigma_f^{\text{U}-235}$.

From Eq. (7), it can be seen that the calculation of the single-group cross-section is directly related to the neutron spectrum, highlighting that the neutron spectrum governs the magnitude of the cross-section. Furthermore, variations in the spectrum are primarily driven by fuel loading, underscoring an intrinsic link between the spectrum and uranium concentration. As uranium concentration increases, neutron absorption strengthens, which diminishes the moderator capacity of the fuel salt, resulting in spectrum hardening, as shown in Fig. 3(a). Establishing the relationship between neutron spectrum and uranium concentration is a challenging task that requires solving for the neutron spectrum. If the free gas model is applied, the neutron spectrum follows a Maxwell-Boltzmann distribution. However, due to the continuous generation of fission neutrons and their absorption by the medium during moderation, the neutron spectrum shifts toward higher energies [42]. The approach in this work avoids seeking analytical solutions for the neutron energy spectrum and subsequently applying Eq. (7) to determine for the fission cross-section. Instead, neutron transport calculations are directly employed to obtain the energy spectrum. Single-group cross-sections are processed to establish their relationship with uranium concentration. This aspect of the work is accomplished using SCALE 6.1. A fitting analysis has been conducted to examine the relationship between $\sigma_f^{\text{U}-235}$ and $M_{\text{U}-235}$, and the results indicate that $1/\sigma_f^{\text{U}-235}$ and $M_{\text{U}-235}$ exhibit a highly linear relationship, with a linear determination coefficient R^2 reaching as high as 0.99998. This linear relationship can be described as:

$$\frac{1}{\sigma_f^{\text{U}-235}} = c_3 M_{\text{U}-235} + c_4 \tag{11}$$

In Eq. (11), c_3 and c_4 are respectively the slope and intercept of the linear fit, which are constants. The results of the linear fit are shown in Fig. 5. Qualitatively, for Eq. (11), as the amount of uranium increases, the neutron energy spectrum hardens, and the single-group fission cross-section decreases. The linear relationship may be related to the 1/v law for the fission cross-section in the thermal neutron energy region, and the theoretical methods based on the energy spectrum still need further exploration.

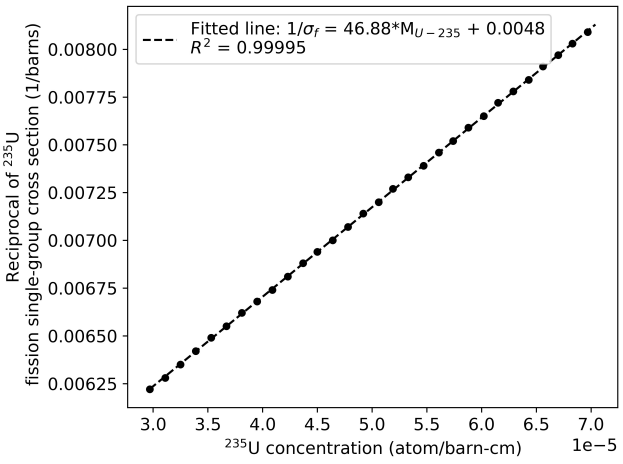

Fig. 5. (Color online) Linear fit of the reciprocal of the ^{235}U fission cross-section with concentration.

Substituting Eq. (11) into Eq. (10) allows for further simplification of Eq. (10), resulting in:

$$\begin{aligned} k_{\text{eff}} &= \frac{M_{\text{U}-235}}{a + bM_{\text{U}-235}}, \\ a &= (\sum c_1^i M_i - c_4 \sum c_2^i M_i)/\nu, \\ b &= (c_3 \sum c_2^i M_i + c_1^{\text{U}-235} + wc_1^{\text{U}-238})/\nu \end{aligned} \tag{12}$$

In Eq. (12), k_{eff} depends solely on the concentration of ^{235}U. If the reciprocal is taken on both sides of Eq. (12), resulting in Eq. (5), it demonstrates that $1/k_{\text{eff}}$ or reactivity

($\rho = 1 - 1/k_{\text{eff}}$) is linearly related to the reciprocal of the uranium concentration. From this, it can be seen that the slope and intercepts a and b of the linear relationship between reactivity and the reciprocal of M_{U-235} are mainly related to the linear relationships between the cross-sections c_1^i and c_2^i, as well as the linear relationship between the reciprocal of the cross-sections and M_{U-235}, c_3 and c_4. In other words, the better the linear relationships in Eq. (8) and Eq. (12), the better the linear relationship in Eq. (5).

It can be observed that from Eq. (6) to Eq. (2), we have made several approximations. These approximations are summarized as follows:

1. The single-group absorption cross-section of the main nuclide is linearly related to the single-group fission cross-section of ^{235}U, as shown in Fig. 4 or Eq. (8). The absorption cross-sections of ^{235}U and ^{238}U approximately have a proportional relationship to the ^{235}U fission cross-section.

2. $1/\sigma_f^{U-235}$ exhibits a linear relationship with M_{U-235}, as shown in Fig. 5 or Eq. (11).

3. Exclude the contribution from ^{238}U fission.

4. Exclude changes in concentrations of other nuclides besides uranium.

5. The average number of neutrons per fission, υ, is constant.

V. VALIDATION OF APPLICABILITY

In the previous section, we utilized the single lattice model illustrated in Fig. 1(b) to justify the validity of Eq. (5). By analyzing the variation of single-group cross-sections with changes in uranium concentration and applying reasonable approximations, we successfully demonstrated the linear relationship between reactivity and the reciprocal of uranium concentration. However, as shown in Fig. 1(a), in the typical core structure of a reactor, apart from the core's active region, there are also reflector layers and various structural materials. These materials absorb neutrons to varying degrees and alter the neutron energy spectrum. Nevertheless, since these structures remain unchanged with variations in uranium concentration, similar to the single lattice structure, they can be physically equivalent to a graphite moderation structure. Therefore, Eq. (5) or Eq. (12) should remain valid in the core model. To validate this conclusion, we simulate and compute the variation of k_{eff} with uranium concentration in the core model.

A. Verification of the linear relationship

Firstly, based on the core model in Fig. 1(a), we verify the linear relationship between $1/k_{\text{eff}}$ and 1/ M_{U-235} under the condition that the volume fraction (VF) and uranium enrichment (wt) of the molten salt channel in the single-lattice model are the same (i.e., VF equals 15%, and wt equals 20%). Simultaneously, the uranium concentration is expanded from 0.02-1 mol% to 0.02-3 mol%. The purpose of this part of the section is to demonstrate the applicability of the aforementioned linear relationship within the core model.

The method involves using SCALE6.1 to calculate the k_{eff} of the reactor at different uranium concentrations and to establish the relationship between reactivity and uranium concentration. As shown in Fig. 6(a), $1/k_{\text{eff}}$ exhibits a highly linear relationship with the reciprocal of uranium concentration ($1/M_{U-235}$). The fitted coefficient of determination R^2 is 0.99995, very close to 1. Furthermore, with ^{235}U concentrations ranging from 1.4E-6 to 2.0E-4 atoms/b-cm, the k_{eff} values span from 0.08 to 1.43, covering nearly all possible fuel loading scenarios. This verifies the conclusion that the reactivity, derived from the single-lattice model, is linearly related to the reciprocal of the uranium concentration.

To further illustrate the accuracy of the aforementioned linear relationship, Fig. 6(b) presents the statistical error in calculating k_{eff} directly by the SCALE6.1 program, as well as the relative deviation between k_{eff} derived from the linear relationship in Fig. 6(a) and the results calculated by SCALE6.1 (i.e., the difference between the k_{eff} values obtained by the two methods). From Fig. 6(b), it can be observed that the error in calculating k_{eff} by SCALE6.1 is essentially maintained between approximately 30 to 50 pcm. Although the relative deviation between the k_{eff} calculated through the linear relationship in Fig. 6(a) and that of SCALE6.1 fluctuates more significantly, within the range of k_{eff} from 0.7 to 1.1, the deviation is essentially within $\pm$100 pcm. Therefore, Fig. 6(b) directly demonstrates the accuracy of calculating k_{eff} through the linear relationship shown in Fig. 6(a), within the allowable error range.

B. Impact of molten salt volume fraction (VF)

In the process of deriving the linear relationship, the most important approximation used is that the neutron absorption cross sections of all nuclides are linearly related to the fission cross section of ^{235}U, represented by approximation condition (1). The main rationale for this approximation is that in graphite-moderated molten salt reactors, the neutron energy spectrum is thermal, which diminishes the impact of resonance absorption and fast neutron absorption reactions. When the fuel composition is the same, the neutron spectrum is primarily influenced by the proportion of molten salt volume within the graphite channels. This section discuss primarily the applicability of the aforementioned linear relationship under different volume fraction (VF) conditions. The method of verification involves keeping the enrichment of ^{235}U constant at 20 wt% and calculating the relationship between k_{eff} and uranium concentration at different VF using SCALE6.1. The range of VF is from 5% to 40%.

Firstly, observe how the neutron energy spectrum changes as VF varies. Fig. 7 shows the normalized neutron flux distribution as a function of energy for different VF values. At different VF values, with the uranium loading remaining con-

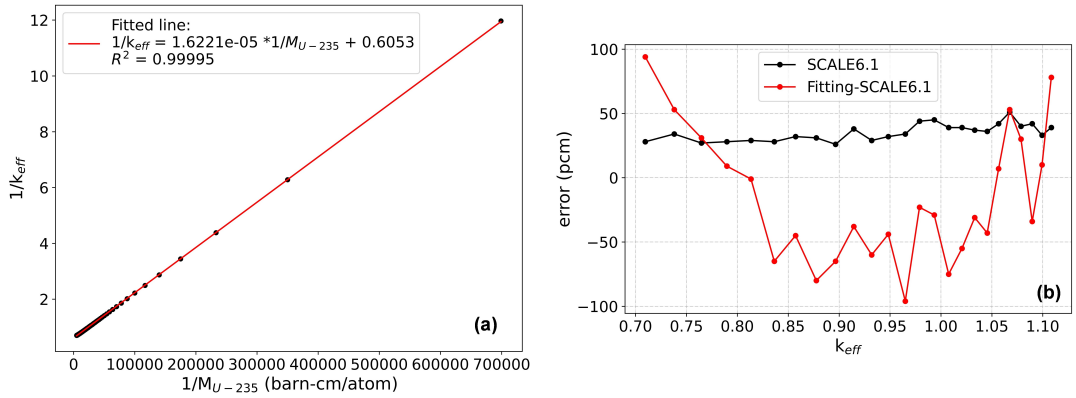

Fig. 6. (Color online) Linear relationship between $1/k_{\mathrm{eff}}$ and $1/\mathrm{M}_{\mathrm{U-235}}$(a), accuracy of k_{eff} calculated by linear regression(b).

stant, the corresponding concentration of ^{235}U is 3.81E-05 atom/barn-cm. For VF=15%, k_{eff}=1. Fig. 7 shows that the neutron energy spectrum undergoes significant changes as VF varies. The main effect is that as VF increases, the neutron flux decreases in the thermal region (E $<$ 1eV), while correspondingly, the neutron flux increases in the intermediate and fast neutron energy regions. Combining the neutron absorption cross-sections of various nuclides from Fig. 3(a), it can be seen that the relative increase in neutron flux in the resonance or fast neutron energy regions leads to a relative decrease in neutrons that conform to the 1/v law. As a result, this will inevitably degrade the linearity between the absorption cross-sections of various nuclides and the fission cross-section of ^{235}U, meaning that the approximate condition (1) no longer holds. Ultimately causing deviation from a linear relationship between reactivity and $1/\mathrm{M}_{\mathrm{U-235}}$.

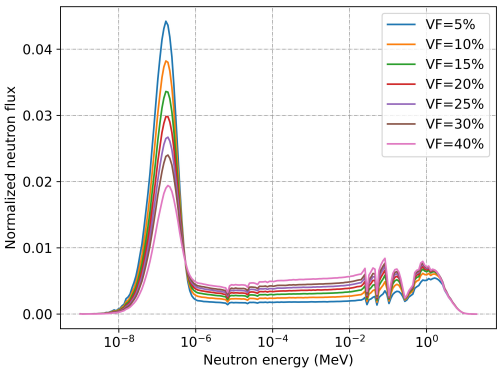

Fig. 7. (Color online) Normalized neutron energy spectrum at different volume fractions (VF).

Fig. 8(a) shows the local curves of the relationship between $1/k_{\mathrm{eff}}$ and $1/\mathrm{M}_{\mathrm{U-235}}$ at different VF values. It can be observed that as VF increases, the curve gradually bends, with a more pronounced bend at higher VF values. Correspondingly, as VF increases, the determination coefficient R^2 of the linear fit between $1/k_{\mathrm{eff}}$ and $1/\mathrm{M}_{\mathrm{U-235}}$ gradually decreases, which means it deviates increasingly from the linear relationship. Fig. 8(a) directly illustrates that an increase in VF, or the hardening of the neutron energy spectrum, leads to a deviation from the linear relationship between reactivity and the reciprocal of uranium concentration. This deviation is a gradual change with the variation of VF, and the applicability of the linear relationship does not have a strict limit, it is mainly related to the error requirements. Generally speaking, for a graphite-moderated molten salt reactor, the optimal design range for VF is 10-20% [40, 43, 44]. Within this range, the determination coefficient is above 0.9999, indicating a highly linear relationship between reactivity and the reciprocal of uranium concentration.

C. Impact of uranium enrichment

As shown in Fig. 3(a), ^{238}U has strong resonance capture cross-sections, and its varying content in the fuel salt may result in different relationships between reactivity and uranium concentration. Furthermore, to validate the applicability range of the linear relationship in Eq. (3), we continue studying the relationship between reactor reactivity and uranium concentration under various uranium enrichments. The verification method involves keeping the VF constant at 15% and using SCALE6.1 to calculate the relationship between k_{eff} and uranium concentration under different enrichments of ^{235}U. In the study, the enrichment range of ^{235}U in UF_4 ranges from 4 to 20 wt%, and the effect of enrichment variation on the density of UF_4 is neglected during the calculation.

Fig. 8(b) shows the relationship between $1/k_{\mathrm{eff}}$ and the reciprocal of uranium concentration at different uranium enrichments, along with the determination coefficient R^2 obtained from linear fitting. From Fig. 8(b), it is evident that within the range of 4-20 wt% uranium enrichment, there is a strong linear correlation between $1/k_{\mathrm{eff}}$ and $1/\mathrm{M}_{\mathrm{U-235}}$, with no deviation from linearity as observed in Fig. 8(a). The linear correlation coefficients for different enrichment are all greater than 0.99995, demonstrating the applicability of this linear relationship across varying enrichment conditions. Although the determination coefficients exhibit slight fluctuations, all values exceed 0.99995, indicating that the fluctuations are within the computational precision of the linear fit-

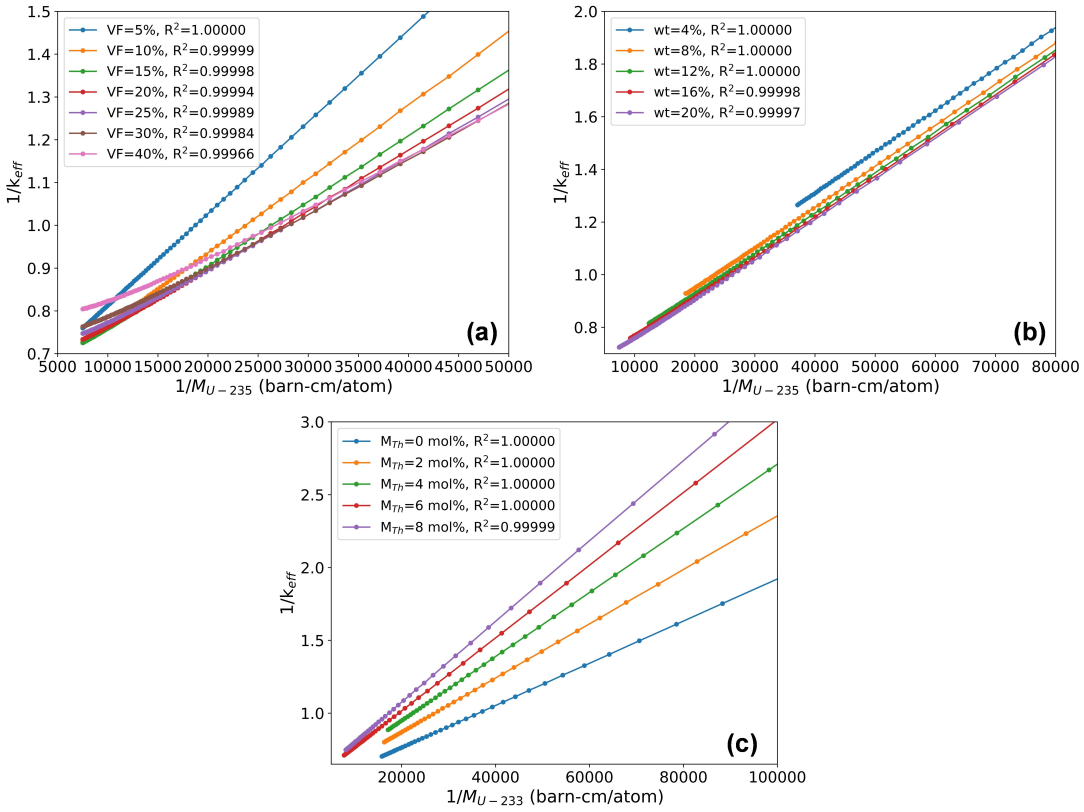

Fig. 8. (Color online) Relationship curves of $1/k_{\text{eff}}$ versus $1/\text{M}_{\text{U}-235}$ at different volume fractions (a), different uranium enrichments(b), different thorium loads(c).

ting and can be attributed to computational errors. Therefore, we conclude that under various low-enriched uranium conditions, a strong linear relationship exists between reactivity and the reciprocal of uranium concentration. The reason for this is that despite the several-fold variation in uranium enrichment, the overall absorption cross-section of ^{238}U is much smaller compared to the fission cross-section of ^{235}U [45]. Thus, the change in enrichment does not significantly affect the calculation of k_{eff} using Eq. (6). In contrast, changes in the volume fraction (VF) have a more pronounced impact, altering the neutron spectrum and affecting the neutron absorption cross-sections of all isotopes, including ^{238}U. Consequently, when VF becomes too large, nonlinear deviations from the linear relationship occur. Additionally, comparing Fig. 8(a) and Fig. 8(b), it is observed that the intercept of the linear fit varies with uranium enrichment, while the slope remains nearly constant. However, under different VF values, both the intercept and slope change. This can be explained by Eq. (12). When uranium enrichment changes, the neutron energy spectrum varies only slightly, so c_i does not change significantly, and consequently, the slope (a) remains relatively stable. However, the intercept (b) is related to the enrichment level and thus changes accordingly. When VF changes, the neutron energy spectrum undergoes significant changes, leading to variations in c_i, which in turn affect both the slope and intercept.

D. ^{232}Th/^{233}U fuel

Based on the analysis of ^{235}U/^{238}U fuel, the primary reason for the linear relationship between reactivity and the reciprocal of uranium concentration is that, in the thermal neutron energy region, the neutron absorption cross-sections of the main nuclides follow the 1/v law. The fission cross-section of ^{233}U is similar to that of ^{235}U and also adheres to the 1/v law. Therefore, the same linear relationship observed in the analysis should also apply to ^{232}Th/^{233}U fuel. To verify this conclusion, the relationship between reactivity and concentration is examined using ^{232}Th/^{233}U fuel. Using the core model shown in Fig. 1(a), the fuel salt composition is 67LiF-33BeF_2-(0-8)ThF_4-xUF_4 (mol%). The ThF_4 content ranges from 0 to 8 mol%, aiming to validate the applicability of the linear relationship under different thorium loading conditions. Reactivity is adjusted by varying the amount of UF_4 (i.e., the value of x) under different thorium loadings. The verification results, shown in Fig. 8(c), demonstrate that $1/k_{\text{eff}}$ and $1/\text{M}_{\text{U}-233}$ exhibit a strong linear relationship under different thorium loadings. This confirms the applicability of this linear relationship to ^{232}Th/^{233}U fuel.

VI. CONCLUSION

Due to its liquid fuel characteristics, the graphite-moderated molten salt reactor considers the fuel loading process as equivalent to increasing the uranium concentration in the fuel salt. There exists a corresponding relationship between uranium loading or concentration and reactivity. The paper first investigates the variation of neutron spectrum and reaction cross-sections with uranium concentration using a single lattice cell model. Under certain approximations, it derives a linear relationship between reactivity and the reciprocal of uranium concentration based on neutron balance theory. Subsequently, the applicability of this linear relationship is validated through simulation calculations using a core model. Based on these studies, the following main conclusions are drawn:

1. Due to the thermal neutron spectrum in graphite-moderated molten salt reactors, and the fact that at low energies the neutron absorption cross-sections of various nuclides follow the 1/v law, it is concluded that the neutron single-group absorption cross-sections of each nuclide approximately exhibit a linear relationship with the single-group fission cross-section of ^{235}U.

2. The reciprocal of the ^{235}U single-group fission cross-section is linearly related to the uranium concentration.

3. The reactor reactivity is linearly related to the reciprocal of uranium concentration, a conclusion drawn on the basis of the two aforementioned premises and also the main conclusion that this paper aims to demonstrate.

4. In conclusion (3), the linear relationship weakens as the volume fraction of graphite molten salt channels increases. However, within the optimal design range of VF=10-20%, the coefficient of determination (R^2) for this linear relationship remains greater than 0.9999, indicating a high degree of linearity.

5. In conclusion (3), the linear relationship, within the range of ^{235}U enrichment from 4-20 wt%, is minimally affected by uranium enrichment. At VF=15%, the linear coefficient of determination remains above 0.99995 across different enrichments, demonstrating a highly linear relationship.

6. For ^{232}Th/^{233}U fuel, this linear relationship still holds highly.

The relationship between reactor reactivity and the loading of nuclear fuel is generally considered to be complex. When the loading of nuclear fuel changes, it usually requires complex transport calculations, which are time-consuming and labor-intensive, to determine the impact. During the fuel loading process in experiments, reactors are often in a subcritical or deep subcritical state, making measurements of reactivity challenging. This paper establishes a simple relationship between reactivity and uranium concentration through simulation analysis, which can be used for calculating or measuring reactor reactivity. Moreover, it effectively establishes a connection between the amount of nuclear fuel loaded and reactivity, applicable in numerous scenarios such as critical extrapolation during the fuel loading process. This research on the relationship between reactor reactivity and uranium concentration has established a simple linear relationship through theoretical analysis and simulation verification. This relationship has significant application value in both theoretical analysis and engineering experiments of molten salt reactors. Additionally, it should be noted that the reactor model used in this paper is a single-zone structure, meaning all lattices have the same VF. For molten salt reactors with more complex partition designs, the relationship between reactivity and uranium concentration may take different forms and requires further validation.

ACKNOWLEDGMENTS

Thanks to the Chinese Academy of Sciences and all sectors of society for their support in the development of molten salt reactors.

AUTHOR CONTRIBUTIONS

Changqing Yu oversees the conceptualization, writing, and data analysis of the article, while Guifeng Zhu contribute to the funding, conceptualization and writing. Jia Shuyang makes significant contributions to the revision of articles. Zou Yang, Rui Yan, Jian Guo, Yafen Liu, Bo Zhou, Xuechao Zhao provide suggestions for analysis and assist with writing revisions.

[1] ABRAM T J. A Technology Roadmap for Generation-IV Nuclear Energy Systems, USDOE/GIF-002-00, F, 2002 [C].

[2] SCHULENBERG T. Molten Salt Reactors [M]//SCHULENBERG T. The fourth generation of nuclear reactors: Fundamentals, Types, and Benefits Explained. Berlin, Heidelberg; Springer Berlin Heidelberg. 2022: 147-65.

[3] LI X-X, CUI D-Y, ZOU C-Y, et al. Assembly-level analysis on temperature coefficient of reactivity in a graphite-moderated fuel salt reactor fueled with low-enriched uranium [J]. Nuclear Science and Techniques, 2023, 34(5): 70.doi:10.1007/s41365-023-01216-0.

[4] WEN G-A, WU J-H, ZOU C-Y, et al. Preliminarysafety analysis for a heavy water-moderated molten salt reactor [J]. Nuclear Science and Techniques, 2024, 35(6): 106.doi:10.1007/s41365-024-01476-4.

[5] ZHAO X-C, YAN R, ZHU G-F, et al. Plutonium utilization in a small modular molten-salt reactor based on a batch fuel reprocessing scheme [J]. Nuclear Science and Techniques, 2024, 35(4): 68.doi:10.1007/s41365-024-01428-y.

[6] ZUO X-D, CHENG M-S, DAI Y-Q, et al. Flow field effect of delayed neutron precursors in liquid-fueled molten salt reactors [J]. Nuclear Science and Techniques, 2022, 33(8): 96.doi:10.1007/s41365-022-01084-0.

[7] HE L-Y, CUI Y, CHEN L, et al. Effect of reprocessing on neutrons of a molten chloride salt fast reactor [J]. Nuclear Science and Techniques, 2023, 34(3): 46.doi:10.1007/s41365-023-01186-3

[8] ZOU C, YU C, ZHOU J, et al. Minor Actinides Transmutation in Thermal, Epithermal and Fast Molten Salt Reactors with Very Deep Burnup; proceedings of the Proceedings of the 23rd Pacific Basin Nuclear Conference, Volume 1, Singapore, F 2023//, 2023 [C]. Springer Nature Singapore.

[9] LIU S, CAI J. Studies of fuel loading pattern optimization for a typical pressurized water reactor (PWR) using improved pivot particle swarm method [J]. Annals of Nuclear Energy, 2012, 50: 117-25.doi:https://doi.org/10.1016/j.anucene.2012.08.007

[10] LINDAUER R B. MSRE DESIGN AND OPERATIONS REPORT. PART VII. FUEL HANDLING AND PROCESSING PLANT [R]. United States, 1965.

[11] ROPER R, HARKEMA M, SABHARWALL P, et al. Molten salt for advanced energy applications: A review [J]. Annals of Nuclear Energy, 2022, 169: 108924.doi:https://doi.org/10.1016/j.anucene.2021.108924

[12] DAI Z. 17 - Thorium molten salt reactor nuclear energy system (TMSR) [M]//DOLAN T J. Molten Salt Reactors and Thorium Energy. Woodhead Publishing. 2017: 531-40.

[13] SILVA C A M, MAGALHãES I R, LORDUY-ALóS M, et al. A neutronic evaluation of a thorium-based molten salt breeder reactor [J]. Nuclear Engineering and Design, 2024, 421: 113049.doi:https://doi.org/10.1016/j.nucengdes.2024.113049

[14] FIORINA C, AUFIERO M, CAMMI A, et al. Investigation of the MSFR core physics and fuel cycle characteristics [J]. Progress in Nuclear Energy, 2013, 68: 153-68.doi:https://doi.org/10.1016/j.pnucene.2013.06.006

[15] IGNATIEV V, FEYNBERG O, GNIDOI I, et al. Molten salt actinide recycler and transforming system without and with Th–U support: Fuel cycle flexibility and key material properties [J]. Annals of Nuclear Energy, 2014, 64: 408-20.doi:https://doi.org/10.1016/j.anucene.2013.09.004

[16] KREPEL J, KRAMER K J. Chapter 27 - TerraPower fast chloride reactor. This chapter was published in Encyclopedia of Nuclear Energy, Volume 1, Section 3, Chapter 11. Molten Chloride Fast Reactors (MCFRs), Pages 625–642, Copyright Elsevier (2021) [M]//DOLAN T J, PáZSIT I, RYKHLEVSKII A, et al. Molten Salt Reactors and Thorium Energy (Second Edition). Woodhead Publishing. 2024: 953-72.

[17] WANG L, SUN W, XIA B, et al. Preferred core conceptual design of pebble bed advanced high temperature reactor [J]. Annals of Nuclear Energy, 2021, 151: 107983.doi:https://doi.org/10.1016/j.anucene.2020.107983

[18] JIANG D, ZHANG D, LI X, et al. Fluoride-salt-cooled high-temperature reactors: Review of historical milestones, research status, challenges, and outlook [J]. Renewable and Sustainable Energy Reviews, 2022, 161: 112345.doi:https://doi.org/10.1016/j.rser.2022.112345

[19] PRINCE B E, BALL S J, ENGEL J R, et al. ZERO-POWER PHYSICS EXPERIMENTS ON THE MOLTEN-SALT REACTOR EXPERIMENT [R]. United States, 1968.

[20] ROBERTSON R C. MSRE Design & Operations Report Part 1 Description of Reactor Design [R]. United States, 1965.

[21] JING X, XU X, YANG Y, et al. Prediction calculations and experiments for the first criticality of the 10 MW High Temperature Gas-cooled Reactor-Test Module [J]. Nuclear Engineering and Design, 2002, 218(1): 43-9.doi:https://doi.org/10.1016/S0029-5493(02)00184-X

[22] BYKHUN A, GLADKIKH P, KARNAUKHOV I, et al. Reactivity Measurement Methods and the First Results of the Physical Start-up for the Nuclear Subcritical Facility “Neutron Source” [J]. Ukrainian Journal of Physics, 2023, 68: 147.doi:10.15407/ujpe68.3.147

[23] BAI J, WAN C, HONG S G, et al. A practical subcritical rod worth measurement technique based on the improved neutron source multiplication method [J]. Nuclear Engineering and Technology, 2024, 56(4): 1398-406.doi:https://doi.org/10.1016/j.net.2023.11.044

[24] SHI Y-Q, ZHU Q-F, TAO H. Review and Research of the Neutron Source Multiplication Method in Nuclear Critical Safety [J]. Nuclear Technology, 2005, 149(1): 122-7.doi:10.13182/NT05-2

[25] DINIZ R C, ROSA F S D S D, GONçALVES A D C. Reactivity calculation in molten salt reactors with inverse kinetics model [J]. Annals of Nuclear Energy, 2023, 194: 110130.doi:https://doi.org/10.1016/j.anucene.2023.110130

[26] JIANG W, ZHU Q-F, ZHOU Q, et al. Reactivity worth measurement of the lead target on VENUS-II light water reactor and validation of evaluated nuclear data [J]. Annals of Nuclear Energy, 2022, 165: 108779.doi:https://doi.org/10.1016/j.anucene.2021.108779

[27] TRUCHET G, VAN ROOIJEN W F G, SHIMAZU Y, et al. Application of the modified neutron source multiplication method to the prototype FBR Monju [J]. Annals of Nuclear Energy, 2013, 51: 94-106.doi:https://doi.org/10.1016/j.anucene.2012.07.040

[28] WANG W, LIU C, HUANG L. The first application of modified neutron source multiplication method in subcriticality monitoring based on Monte Carlo [J]. Nuclear Engineering and Technology, 2020, 52(3): 477-84.doi:https://doi.org/10.1016/j.net.2019.08.014

[29] ASHRAF O, TIKHOMIROV G V. Preliminary study on the online reprocessing and refueling scheme for SD-TMS reactor [J]. Journal of Physics: Conference Series, 2020, 1439(1): 012005.doi:10.1088/1742-6596/1439/1/012005

[30] XIA S, CHEN J, GUO W, et al. Development of a Molten Salt Reactor specific depletion code MODEC [J]. Annals of Nuclear Energy, 2019, 124: 88-97.doi:https://doi.org/10.1016/j.anucene.2018.09.032

[31] GUI-FENG Z H U, YANG Z O U, MING-HAI L I, et al. Development of Burnup Calculation Code for Pebble-bed High Temperature Reactor at Equilibrium State [J]. Atomic Energy Science and Technology, 2015, 49(5): 890-6.doi:10.7538/yzk.2015.49.05.0890

[32] FIEL J C B. Neutronic calculations of a thermal reactor using the Albedo Method in two energy groups [J]. Annals of Nuclear Energy, 2018, 115: 83-7.doi:https://doi.org/10.1016/j.anucene.2018.01.002

[33] JANZ G J. Thermodynamic and transport properties for molten salts : correlation equations for critically evaluated density, sur-

face tension, electrical conductance, and viscosity data, F, 1988 [C].
[34] WILLIAMS D F. Assessment of Candidate Molten Salt Coolants for the NGNP/NHI Heat-Transfer Loop [R]. United States, 2006.
[35] PARK J, LEONG A, ZHANG J. Density Measurements of Molten Salts [J]. Journal of Chemical & Engineering Data, 2023, 68(8): 1892-8.doi:10.1021/acs.jced.3c00171
[36] BOWMAN S M. SCALE 6: Comprehensive Nuclear Safety Analysis Code System [J]. 2011, 174: Medium: X; Size: 126-48.doi:10.13182/nt10-163
[37] BO Z, YU X-H, ZOU Y, et al. Study on dynamic characteristics of fission products in 2 MW molten salt reactor [J]. Nuclear Science and Techniques, 2020, 31.doi:10.1007/s41365-020-0730-z
[38] CHEN L, YAN R, KANG X-Z, et al. Study on the production characteristics of 131I and 90Sr isotopes in a molten salt reactor [J]. Nuclear Science and Techniques, 2021, 32.doi:10.1007/s41365-021-00867-1
[39] THOMAS P. 21 - Nuclear reactors [M]//THOMAS P. Simulation of Industrial Processes for Control Engineers. Oxford; Butterworth-Heinemann. 1999: 268-81.
[40] TAN M-L, ZHU G-F, ZHANG Z-D, et al. Burnup optimization of once-through molten salt reactors using enriched uranium and thorium [J]. Nuclear Science and Techniques, 2022, 33(1): 5.doi:10.1007/s41365-022-00995-2
[41] YU C, ZHU G, LIU Y, et al. Comparative Study on the Neutronic Performance of Thermal and Fast Molten Salt Reactors under Once-Through Fuel Cycle [J]. 2023, 2023(1): 8875215.doi:https://doi.org/10.1155/2023/8875215
[42] MARGUET S. Thermalization of Neutrons [M]//MARGUET S. The Physics of Nuclear Reactors. Cham; Springer International Publishing. 2017: 387-463.
[43] KANG X, GUIFENG Z, WU J, et al. Core Optimization for Extending the Graphite Irradiation Lifespan in a Small Modular Thorium-Based Molten Salt Reactor [J]. Journal of Nuclear Engineering, 2024, 5: 16.doi:10.3390/jne5020012
[44] ZOU C-Y, CAI X Z, JIANG D, et al. Optimization of temperature coefficient and breeding ratio for a graphite-moderated molten salt reactor [J]. 2015, 281: 114-20
[45] TAN M-L, GUIFENG Z, ZOU Y, et al. Research on the effect of the heavy nuclei amount on the temperature reactivity coefficient in a small modular molten salt reactor [J]. Nuclear Science and Techniques, 2019, 30.doi:10.1007/s41365-019-0666-3